Bioconjugate Chemistry

Article

pubs.acs.org/bc

Rationally Engineering Phototherapy Modules of Eosin-Conjugated Responsive Polymeric Nanocarriers via Intracellular Endocytic pH Gradients

Guhuan Liu, Jinming Hu, Guoying Zhang, and Shiyong Liu*

CAS Key Laboratory of Soft Matter Chemistry, Hefei National Laboratory for Physical Sciences at the Microscale, Collaborative Innovation Center of Chemistry for Energy Materials, Department of Polymer Science and Engineering, University of Science and Technology of China, Hefei, Anhui 230026, China

Supporting Information

ABSTRACT: Spatiotemporal switching of respective phototherapy modes at the cellular level with minimum side effects and high therapeutic efficacy is a major challenge for cancer phototherapy. Herein we demonstrate how to address this issue by employing photosensitizer-conjugated pH-responsive block copolymers in combination with intracellular endocytic pH gradients. At neutral pH corresponding to extracellular and cytosol milieu, the copolymers self-assemble into micelles with prominently quenched fluorescence emission and low $^1O_2$ generation capability, favoring a highly efficient photothermal module. Under mildly acidic pH associated with endolysosomes, protonation-triggered micelle-to-unimer transition results in recovered emission and enhanced photodynamic $^1O_2$ efficiency, which synergistically actuates release of encapsulated drugs, endosomal escape, and photochemical internalization processes.

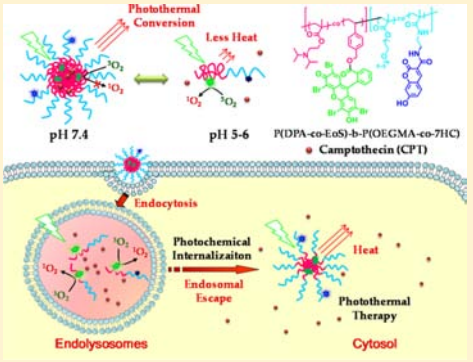

INTRODUCTION

Photodynamic therapy (PDT) has emerged as an important noninvasive cancer treatment technique complementary to chemotherapy and radiotherapy.[1−3] Upon local irradiation of tumor tissues with light of specific wavelength, photosensitizers (PS) are excited and then transfer the energy to oxygen, generating highly reactive oxygen species (e.g., $^1O_2$) which incur vascular damage and direct cytotoxicity. Three prerequisites, i.e., enough oxygen, high PS concentration, and sufficient light dosage, are needed for desired PDT efficacy; however, in metastatic and solid tumors, these conditions are difficult to meet.[4−6] As alternatives, photochemical internalization (PCI) and photothermal therapy (PTT) modules have been proposed. In the PCI process,[7−9] PS is only activated in acidic endosomes and *in situ* generated $^1O_2$ ruptures endosome membranes, accompanied by the escape of therapeutic agents (drugs or genes) into the cytosol before being degraded in lysosomes.[10−15] Hence PCI technique requires much lower oxygen level and lower light dosage than PDT.[16] As an oxygen-independent phototherapy module, PTT is quite applicable to hypoxic tumors. Instead of luminescence emission or transfer to triplet oxygen, the energy of excited PS in PTT mainly transforms into heat via nonradiative decay, which induces temperature elevation and irreversible damage to tumor cells.[17−20] Thus, the therapeutic efficacy of a specific phototherapy module (PDT, PCI, and PTT) strongly depends on the local milieu surrounding the photosensitizer.

Compared to normal ones, pathological sites such as tumor tissues typically exhibit distinct physiological features such as mild acidity (~pH 6.8), overexpressed proteins and enzymes, hypoxia, and high level of metabolites.[21−27] These distinct features have been previously utilized to selectively switch on the PDT module of quenched small molecule PS[28−36] and PS-conjugated nanoparticles.[37−40] For example, PDT potency of chlorin e6-functionalized 3-diethylamino-propyl chitosan nanoparticles can be switched on at mildly acidic tumor sites.[37] For photosensitizer and/or drug-loaded polymeric nanocarriers, upon cellular uptake they will be subjected to intracellular pH gradients (pH 5.9−6.2 in early endosomes, pH 5.0−5.5 in late endosomes and lysosomes, and neutral in cytosol) and redox gradients. Previously, these gradients have been explored to actuate fluorescence turn-on for optical imaging[41−47] and site-specific drug release[21,48−56] from polymeric nanoparticles.

Upon light absorption, the exited state energy of PS can decay via three main pathways: fluorescence emission, phosphorescence emission (when oxygen exists, transfer to oxygen to generate $^1O_2$), and nonradiative decay (heat). If both fluorescence and phosphorescence channels are blocked, the PS will work under the photothermal mode, but for small molecule PS, the PTT effect is minimal due to fast heat dissipation via collision with surrounding water molecules. In this context, PS-

Special Issue: Biofunctional Biomaterials: The Third Generation of Medical Devices

Received: November 25, 2014
Revised: December 15, 2014
Published: December 16, 2014

DOI: 10.1021/bc500548r
Bioconjugate Chem. 2015, 26, 1328−1338

Scheme 1. . Schematics of Multifunctional Micelles Self-Assembled from P(DPA-*co*-EoS)-*b*-P(OEGMA-*co*-7HC) Block Copolymers (BP3) Covalently Conjugated with Green-Emitting Photosensitizer (eosin Y; EoS) and pH-Switchable Blue-Emitting 7-Hydroxycoumarin Moieties (7HC) within the pH-Responsive PDPA Block and Hydrophilic POEGMA Block, Respectively[a]

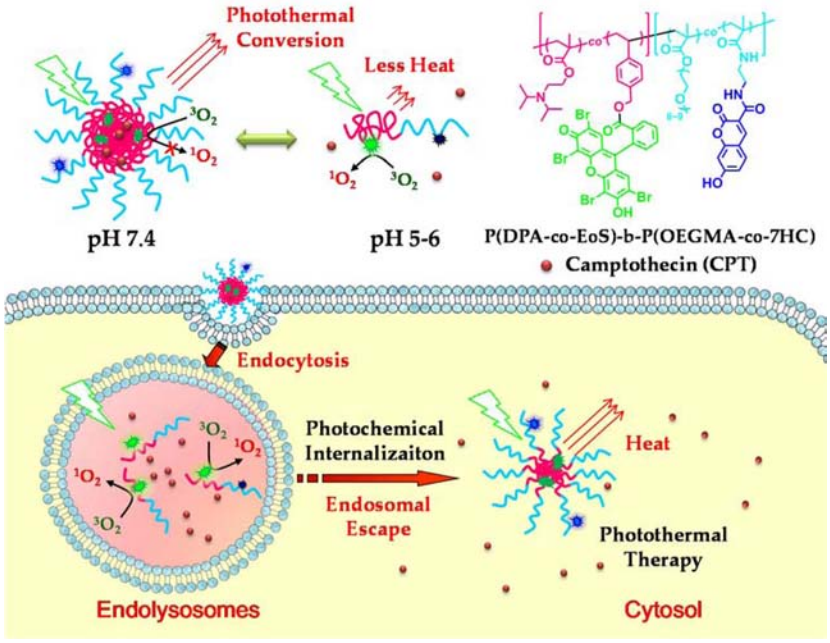

[a]After endocytosis, micelles disintegrate into unimers within acidic endolysosomes and release encapsulated chemotherapeutic drugs. This process is accompanied by the activation of eosin green fluorescence emission and recovery of $^1O_2$ generation efficacy upon light irradiation, whereas 7HC blue emission was suppressed due to the acidic milieu. Subsequently, unimer chains and drugs escape into the neutral cytosol via photochemical internalization (PCI) and reassemble into micelles, restoring the blue emission of 7HC and photothermal therapeutic potency.

Scheme 2. Synthetic Routes Employed[a]

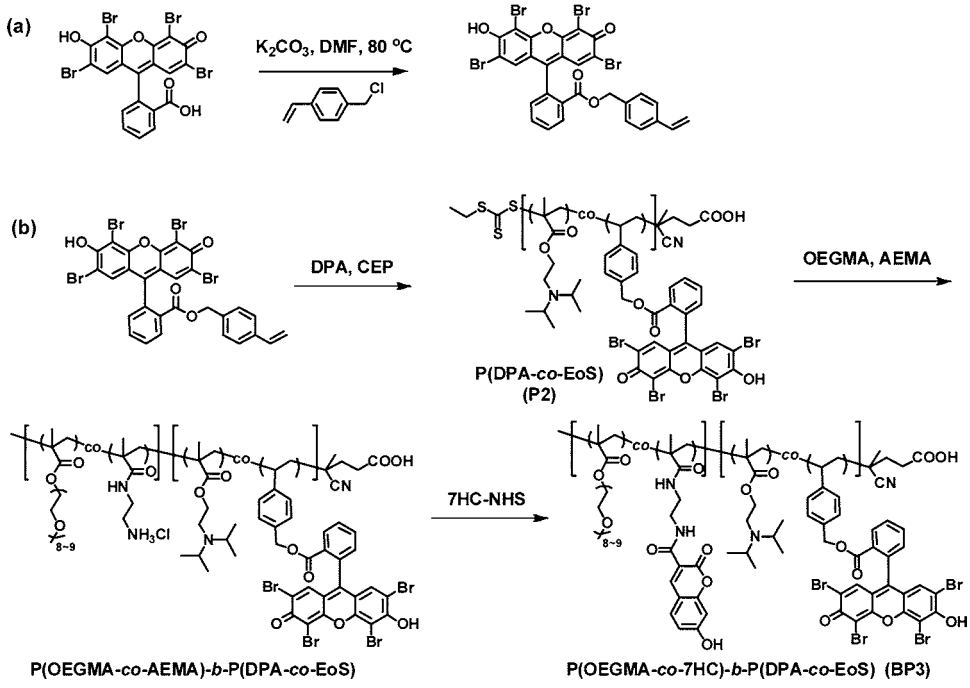

[a]Preparation of (a) eosin-based monomer 4-vinylbenzyl 2-(2,4,5,7-tetrabromo-6-hydroxy-3-oxo-3*H*-xanthen-9-yl)benzoate (EoS) and (b) well-defined P(DPA-*co*-EoS)-*b*-P(OEGMA-*co*-7HC) (**BP3**) DHBC covalently conjugated with green-emitting photosensitizer (eosin moieties; EoS) within the pH-responsive PDPA block and pH-switchable blue-emitting 7-hydroxycoumarin moieties (7HC) in the hydrophilic POEGMA block.

labeled nanoparticles and molecular assemblies show great promise. For example, Zheng and co-workers[57,58] reported porphysomes self-assembled from porphyrin−lipid conjugates. Due to quenched luminescence emission, the excited state

DOI: 10.1021/bc500548r
Bioconjugate Chem. 2015, 26, 1328−1338

energy upon light excitation can only be released thermally, rendering porphysomes excellent PTT agents. However, upon enzymatic release of porphyrin moieties from the conjugates, both photodynamic $^1O_2$ generation efficiency and fluorescence emission were recovered. To the best of our knowledge, it has remained a major challenge to delicately and spatiotemporally modulate respective phototherapy modes at the cellular level according to the local intracellular milieu subjected to nanocarriers during the endocytic pathway.

Herein, we report on the fabrication of pH-switchable phototherapy nanocarriers from P(DPA-*co*-EoS)-*b*-POEGMA double hydrophilic block copolymers (DHBCs, **BP2**) covalently labeled with photosensitizing eosin Y moieties (EoS) within the pH-responsive poly(2-diisopropylaminoethyl methacrylate) (PDPA) block,[41,59] where OEGMA is oligo(ethylene glycol) monomethyl ether methacrylate (Scheme 1). At neutral pH corresponding to blood circulation and the cytosol, **BP2** forms micelles consisting of eosin-labeled PDPA cores and POEGMA coronas. Due to dye self-quenching and PET process between eosin and deprotonated PDPA tertiary amines, the eosin fluorescence emission is quite weak with negligible $^1O_2$ generation, whereas the photothermal potency is highly efficient. Upon endocytosis into endolysosomes (pH ≈ 5.0−6.0), PDPA tertiary amine moieties were protonated and micelle-to-unimer transition occurs, thus blocking the PET process and restoring both fluorescence emission and $^1O_2$ generation efficacy, leading to the spatiotemporal switching of phototherapy modes between PTT in the cytosol and PDT/PCI in endolysosomes. In order to visualize and track PCI-associated endosomal escape process, 7-hydroxycoumarin (7HC) moieties, which are highly fluorescent with blue emission at pH 7.4 and almost nonfluorescent at acidic pH,[60,61] were conjugated onto the POEGMA block of **BP3** DHBCs to act as ratiometric pH imaging probes in combination with pH-switchable eosin emission (Scheme 1).

RESULTS AND DISCUSSION

Dye-labeled DHBCs bearing eosin moieties in the pH-responsive PDPA block and/or 7HC moieties in the hydrophilic POEGMA block were synthesized by combining reversible addition−fragmentation chain transfer (RAFT) polymerization[62−64] and postfunctionalization (**BP1**-**BP3**; Scheme 2 and Supporting Information (SI) Figures S1−S2), and their structural parameters are summarized in Table 1. In

Table 1. Molecular Parameters of Polymer Precursors and Dye-Labeled Double Hydrophilic Block Copolymers (DHBCs)

entry	sample	$M_{n,\,NMR}$[a] (kDa)	$M_{n,\,GPC}$[b] (kDa)	M_w/M_n[b]
P1	$PDPA_{63}$	13.7	15.4	1.19
P2	$P(DPA_{0.95}$-*co*-$EoS_{0.05})_{65}$	16.3	16.7	1.18
BP1	$PDPA_{63}$-*b*-$P(OEGMA$-*co*-$7HC)_{23}$	24.8	28.9	1.22
BP2	$P(DPA_{0.95}$-*co*-$EoS_{0.05})_{65}$-*b*-$POEGMA_{22}$	26.8	30.1	1.23
BP3	$P(DPA_{0.95}$-*co*-$EoS_{0.05})_{65}$-*b*-$P(OEGMA$-*co*-$7HC)_{22}$	26.0	29.7	1.21
BP4	PEG_{113}-*b*-$P(NIPAM$-*co*-$CMA)_{97}$	16.0	15.4	1.13
BP5	PEG_{113}-*b*-$P(NIPAM$-*co*-$NBDAE)_{95}$	15.7	15.8	1.11

[a]Calculated from ^1H NMR results. [b]Determined by GPC using THF as the eluent (1.0 mL/min).

neutral aqueous media, **BP2** self-assembled into spherical micelles as evidenced by TEM observation, and dynamic light scattering (DLS) measurements revealed an intensity-average hydrodynamic diameter, $\langle D_h \rangle$, of ∼22 nm (SI Figure S3). The PDPA block are known to possess a pK_a of ∼6.3; thus, upon decreasing pH micelle-to-unimer transition of **BP2** will occur at ∼pH 6. For eosin-conjugated **BP2** micelles at neutral or alkaline pH, the fluorescence emission is weak due to both dye self-quenching within micellar cores and PET quenching by deprotonated tertiary amines. Upon pH decrease from 10 to 2.5, the emission intensity at 555 nm increased ∼10-fold and most of the changes occurred at around the pK_a (Figure 1b,c). It is noteworthy that in the same pH range, the eosin absorption at 540 nm exhibited a modest decrease (<10%) (Figure 1a).

The capability of **BP2** to modulate singlet oxygen generation in response to external pH stimulus was examined with sacrificial 9,10-aminoethoxyanthracene (*An*-$2NH_2$).[65] The blue-emitting *An*-$2NH_2$ can quantitatively react with $^1O_2$ to generate nonfluorescent anthraquione. Upon green light irradiation of **BP2** solution at varying pH, the *An*-$2NH_2$ emission at 430 nm decreased gradually with extended irradiation duration (SI Figures S4 and S5), implying the generation of $^1O_2$. Apparently, it can be found that the emission intensity of *An*-$2NH_2$ decreased much more slowly at pH 7.4 than at pH 5.0; the degradation rate of *An*-$2NH_2$, i.e., the generation rate of $^1O_2$, at pH 5.0 was ∼5-fold higher than that at pH 7.4 (Figure 1d,f). The photothermal efficiency of the **BP2** micellar system was also examined in the pH range of 4.0−7.4 (Figure 1e). Upon green light irradiation at pH 7.4, the solution temperature increased abruptly and then stabilized at 38.4 °C after 45 min (ambient temperature ∼24 °C), whereas at pH 5.0, the temperature only increased ∼6 °C after being subjected to 45 min green light irradiation. The above results clearly demonstrated the opposite pH-dependence of photodynamic and photothermal potency of **BP2** micelles (Figure 1f), endowing the system with the capability of effecting PTT in the neutral cytosol and PDT/PCI within acidic endolysosomes.

To verify that efficient $^1O_2$ generation within intracellular acidic organelles can aid with endosome escape via PCI effect, **BP3** labeled with both eosin and pH-sensitive 7HC dye (SI Figure S7) were then studied in detail. In the pH range of 3−9, the emission intensity ratio, $I_{447\ nm}/I_{552\ nm}$, dramatically increased from ∼0.045 to 11, i.e., ∼250-fold changes in intensity ratios (Figure 2). The intracellular PCI process of **BP3** micelles was then tracked in human A549 lung cancer cells by confocal laser scanning microscopy (CLSM, Figure 3a). Upon 2 h coincubation with **BP3**, punctuate eosin green-emitting dots appeared inside the cells and most of them colocalized with LysoTracker Red, the marker of late endosomes and lysosomes, whereas the blue 7HC emission was almost undetectable. According to fluorescence pH calibration curve (SI Figure S9), the corresponding pH was calculated to be in the range of 4.8−5.2 (Figure 3b). This confirmed that **BP3** was mainly retained within endolysosomes. The cells were then subjected to green light irradiation for varying time duration and then incubated. The total irradiation and subsequent incubation duration was kept to 2 h. After 10 min light irradiation, green eosin emission remained essentially unchanged and almost colocalized with LysoTracker Red; however, some blue fluorescent dots started to appear and misaligned with those of LysoTracker red. Extending the irradiation time to 30 and 60 min, green dots gradually

DOI: 10.1021/bc500548r
Bioconjugate Chem. 2015, 26, 1328−1338

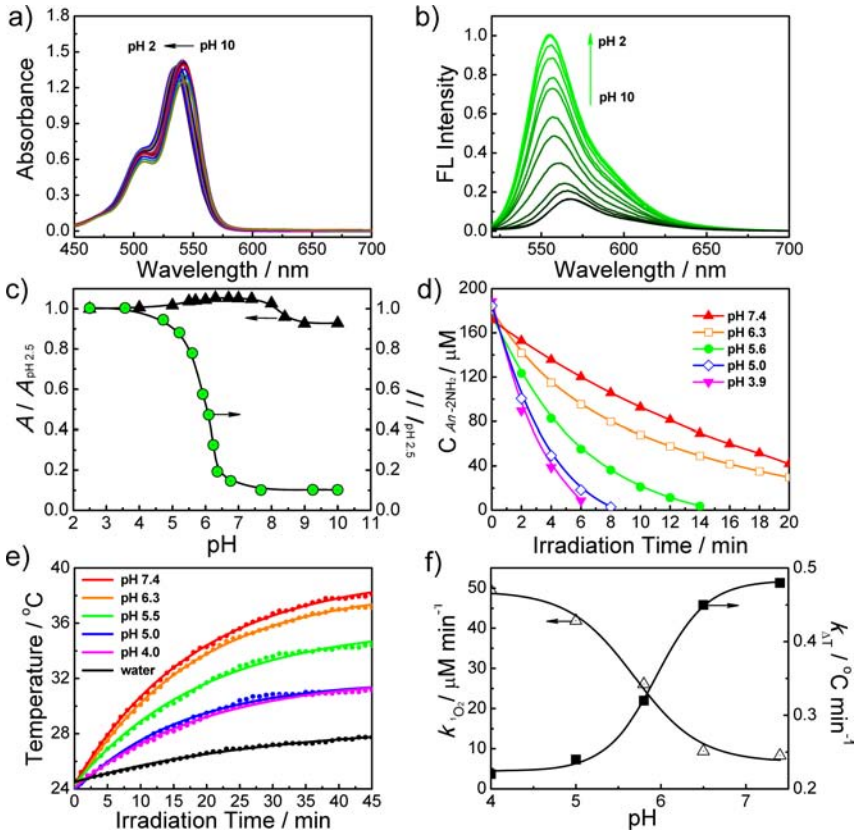

Figure 1. pH-dependent (a) UV−vis absorbance spectra, (b) fluorescence emission spectra (λ_{ex} = 500 nm), and (c) normalized optical absorbance and emission intensities (λ_{em} = 555 nm) at the maximum wavelength recorded for **BP2** aqueous solution. Irradiation duration-dependent (d) *An*-2NH_2 consumption ($^1O_2$ generation) and (e) photothermally triggered temperature increments recorded for oxygen-saturated **BP2** solution (0.5 g/L, 3.5 μM eosin moieties, 25 °C; 520 nm LED light) at varying pH. (f) pH-dependent $^1O_2$ generation rates (decomposition rate of *An*-2NH_2) and temperature elevation rates.

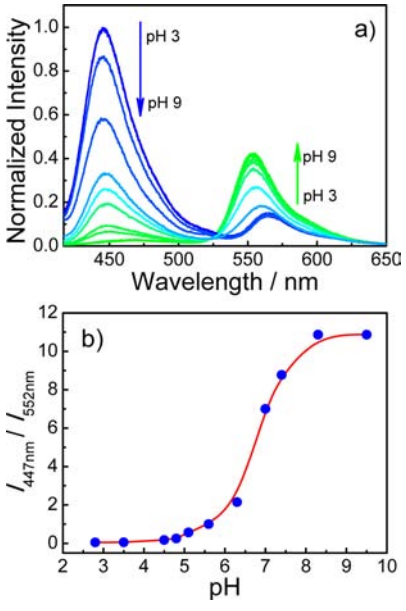

Figure 2. (a) Typical fluorescence emission spectra (λ_{ex} = 400 nm) and (b) normalized emission intensity ratio ($I_{447\ nm}/I_{552\ nm}$) changes recorded for the aqueous solution of **BP3** (0.5 g/L) in the pH range of 3−9.

weakened and disappeared, accompanied by the appearance and strengthening of continuous 7HC blue emission.

Correspondingly, the pH value was determined to be in the range of 6.5−7.5, indicating that **BP3** escaped from lysosomes/endosomes and entered into the cytosol via PCI process. At the same time period, the emission intensity and stained area of LysoTracker Red decreased and finally completely disappeared after 60 min irradiation (Figure 3c). These results confirmed the rupture of acidic endolysosomes induced by PCI under green light irradiation, which can be further evidenced using acridine orange as an intracellular indicator (SI Figure S9).[12,66] The control experiments carried out on A549 cells without green light irradiation or those coincubated with $^1O_2$ scavengers (Vitamin C or *N*-acetyl-L-cysteine, NAC)[29] exhibited no apparent endosomal escape of **BP3** and turn-on of 7HC blue emission (SI Figure S10).

Following the PCI process, **BP2** and **BP3** will enter into the cytosol, where the PTT mode will take effect. To enable intracellular temperature monitoring, we constructed ratiometric fluorescent thermal probes[67] based on two dye-labeled DHBCs, PEG_{113}-*b*-P(NIPAM-*co*-CMA)$_{97}$ (**BP4**) and PEG_{113}-*b*-P(NIPAM-*co*-NBDAE)$_{95}$ (**BP5**) bearing nitrobenzoxadiazole (NBD) and coumarin (CMA) moieties within the thermoresponsive poly(*N*-isopropylacrylamide) (PNIPAM) block, respectively (Figure 4). Upon heating the aqueous mixture of **BP4** and **BP5**, the CMA blue emission at 422 nm exhibited a significant decrease, while the NBD green emission at 525 nm gradually increased. The emission intensity ratio, $I_{525\ nm}/I_{422\ nm}$, increased ~5.5-fold in the range of 30−47 °C (Figure 4c,d).

DOI: 10.1021/bc500548r
Bioconjugate Chem. 2015, 26, 1328−1338

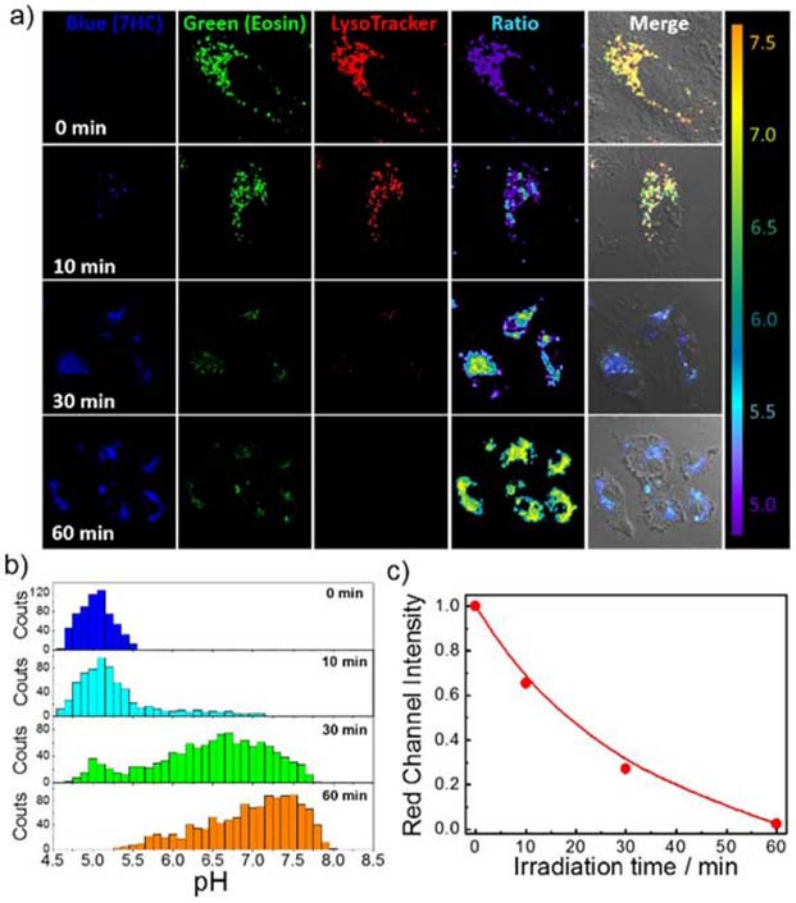

Figure 3. (a) CLSM images recorded at varying irradiation durations (520 nm) for live A549 cells that have been incubated with **BP3** micellar solution for 2 h at 37 °C. Blue, green, and red channel emissions were collected at 450 ± 20 nm, 560 ± 20 nm, and 630 ± 20 nm, respectively; overlay images were from all three channels and ratiometric images were generated from blue to green channel emissions. (b,c) Irradiation duration-dependent evolution of (b) local pH gradient distributions and (c) red channel emission intensities, which were averaged from fluorescence images of multiple cells.

According to the above results (Figure 3), after 2 h coincubation with cells and 30 min green light irradiation, **BP2** could completely escape from endosomes and enter into the cytosol. Fluorescent temperature probes were then added and coincubated with cells for another 1 h at 37 °C. During CLSM experiments, two cells in the square box in Figure 3a were chosen to be irradiated by the 543 HeNe laser for varying number of scans. We can see that within the irradiation area, the green NBD emission increased and blue CMA emission gradually decreased with increasing number of scans (Figure 5a). Based on green/blue emission ratios and temperature calibration curve (SI Figure S11), the intracellular temperature gradient distribution broadened from 36 to 38 °C before laser irradiation to 38−45 °C after 100 times of laser scanning (Figure 5b). Meanwhile, the intracellular temperature outside the irradiation area remained almost unchanged (∼37 °C, Figure 5c). For the control experiments without prior green light irradiation, **BP2** did not escape from endolysosomes via the PCI process, the intracellular temperature gradients of the laser-irradiated area only increased to 37−39 °C after 100 times of scanning (SI Figure S12).

On the other hand, although it is difficult to exactly ascertain at the current stage, we speculate that upon endosomal escape into the cytosol **BP2** chains will reassemble into micelles, as shown in Scheme 1, due to the following reasons.[68] (a) **BP2** unimer chains, like small molecule photosensitizers, can only exhibit quite modest photothermal effects (Figure 1e) due to quick heat dissipation via collision with peripheral water molecules and conformational fluctuations; in addition, fluorescence emission quenching will be weaker for dissolved unimers and this is not advantageous for photothermal heating. However, compared to the unimer state determined for the control, we observed a strong photothermal effect for **BP2** within the cytosol (Figure 5). (b) The overall intracellular concentration is higher than the critical micellization concentration (CMC) of **BP2**, thus upon PCI-induced endosomal escape, local **BP2** concentration within the cytosol should also be above the CMC. (c) For the hydrophobic CPT drug, it will distribute into hydrophobic domains within proteins, other biomacromolecules, and ordered aggregates (i.e., relevant organelles, reformed micelles, or co-micelles involving **BP2**); eventually CPT will tend to accumulate within the nucleolus and interact with DNA to take therapeutic effect.

Next, drug release profiles of CPT-loaded **BP2** micelles were investigated. At pH 7.4 and 37 °C, ∼47% of loaded drug can be released after 25 h; whereas at pH 5.0, the fraction of released drug increased to ∼82% over the same time range (Figure 6a). The enhanced CPT release rate should be ascribed to acid-triggered micelle−unimer transition. In vitro cytotoxicity of **BP2** micelles was examined via the MTT assay against A549 cells (Figure 6b). The cell viability upon 1 h green light irradiation in the absence of **BP2** was ∼85%. For cells

DOI: 10.1021/bc500548r
Bioconjugate Chem. 2015, 26, 1328−1338

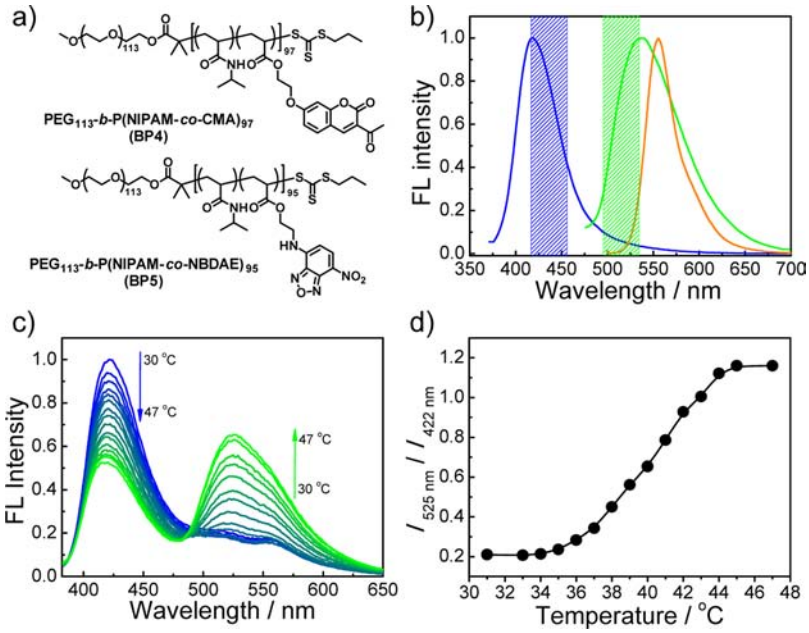

Figure 4. (a) Chemical structures of PEG_{113}-*b*-P(NIPAM-*co*-CMA)$_{97}$ (**BP4**) and PEG_{113}-*b*-P(NIPAM-*co*-NBDAE)$_{95}$ (**BP5**). (b) Fluorescence emission spectra recorded for 0.5 g/L aqueous solutions of **BP4** (blue line, λ_{ex} = 360 nm), **BP5** (green line, λ_{ex} = 460 nm), and **BP2** (red line, λ_{ex} = 480 nm) at 25 °C and pH 5.0. (c) Temperature-dependent fluorescence emission spectra (λ_{ex} = 370 nm) and (d) emission intensity ratio changes ($I_{525\ nm}/I_{422\ nm}$) recorded at pH 7.4 for the aqueous mixture of **BP4** (0.35 g/L), **BP5** (0.15 g/L), and **BP2** (0.2 g/L) in the temperature range of 30−47 °C.

incubated with blank **BP2** micelles (0.02 g/L) and then irradiated with green light for 60 min, the cell viability was ∼42%. Further increasing **BP2** concentration to 0.2 g/L led to a cell viability decrease to ∼20%. This clearly confirmed cytotoxicity exerted via photodynamic and photothermal mechanisms.

Figure 6c,d shows CLSM images recorded for A549 cells after being incubated for 12 h in the presence of CPT-loaded **BP2** micelles with and without 30 min green light irradiation. Without light irradiation, CPT blue emission almost overlapped completely with eosin green emission, confirming the entrapment of both CPT and **BP2** unimers within endolysosomes. However, after 30 min green light irradiation, both CPT and **BP2** will escape from endolysosomes (Figure 3). The blue emission of CPT spread diffusively in the whole cytoplasm and remained separate from that of **BP2** green emission. This indicated extensive release of CPT from **BP2** micelles and this process might well have occurred within acidic endolysosomes (i.e., before endolysosomal escape; Scheme 1). The coincubation of cells with CPT-loaded **BP2** micelles in combination with light irradiation can further promote cell apoptosis. For example, at a polymer concentration of 0.02 g/L, cell viability decreased from ∼42% for blank micelles to ∼18% for CPT-loaded micelles upon 60 min green light irradiation, demonstrating the potency of combined phototherapy and chemotherapy. Figure 4e−h shows CLSM images via Live/Dead staining technique[40,69,70] recorded for A549 cells after being irradiated by green light for 60 min. Compared to the blank control (Figure 6e), the survival rates of cells incubated with CPT-free micelles for 12 h (Figure 6f) and CPT-loaded micelles were much lower, which agreed well with the MTT assay results (Figure 6b). However, when coincubated with Vitamin C as a $^1O_2$ scavenger, the cell survival rate can be largely restored (Figure 6h), implying the important role of $^1O_2$-associated PDT and PCI processes for chemotherapeutic drug/photosensitizer coloaded **BP2** micelles.

■ CONCLUSION

In summary, we fabricated photosensitizer-conjugated responsive block copolymer nanocarriers with pH-switchable phototherapy modules (PDT, PCI, and PTT). In the micellar state at neutral pH corresponding to blood circulation and the cytosol, the eosin luminescence within micellar cores was quenched, associated with low $^1O_2$ generation capability and high photothermal efficacy. Upon cellular internalization, micelle-to-unimer transition occurred within mildly acidic endolysosomes, resulting in recovered fluorescence emission, enhanced photodynamic $^1O_2$ efficiency, and activated PCI process. The latter led to endosome escape and block copolymer reassembly into micelles within the cytosol, where intracellular photothermal heating will take effect. The reported spatiotemporal modulation of respective phototherapy modes at the cellular level in response to pH gradients subjected by block copolymer nanocarriers, and the integration with chemotherapy modality argues well for their future clinical applications in personalized cancer therapy.

■ EXPERIMENTAL SECTION

Materials. Oligo(ethylene glycol) monomethyl ether methacrylate (OEGMA, M_n = 475 g/mol, mean degree of polymerization, DP, is 8−9) purchased from Aldrich was passed through a neutral alumina column to remove the inhibitor and then stored at −20 °C prior to use. *N*,*N*-(Diisopropylamino)ethyl methacrylate (DPA) purchased Aldrich was distilled under vacuum and then stored at −20 °C prior to use. Dioxane, tetrahydrofuran (THF), dimethylfomamide (DMF), and all other reagents were purchased from Sinopharm Chemical Reagent Co. Ltd. and used as received. Eosin Y, 4-chloromethylstyrene, 3-(4,5-dimethylthiazol-2-yl)-

DOI: 10.1021/bc500548r
Bioconjugate Chem. 2015, 26, 1328−1338

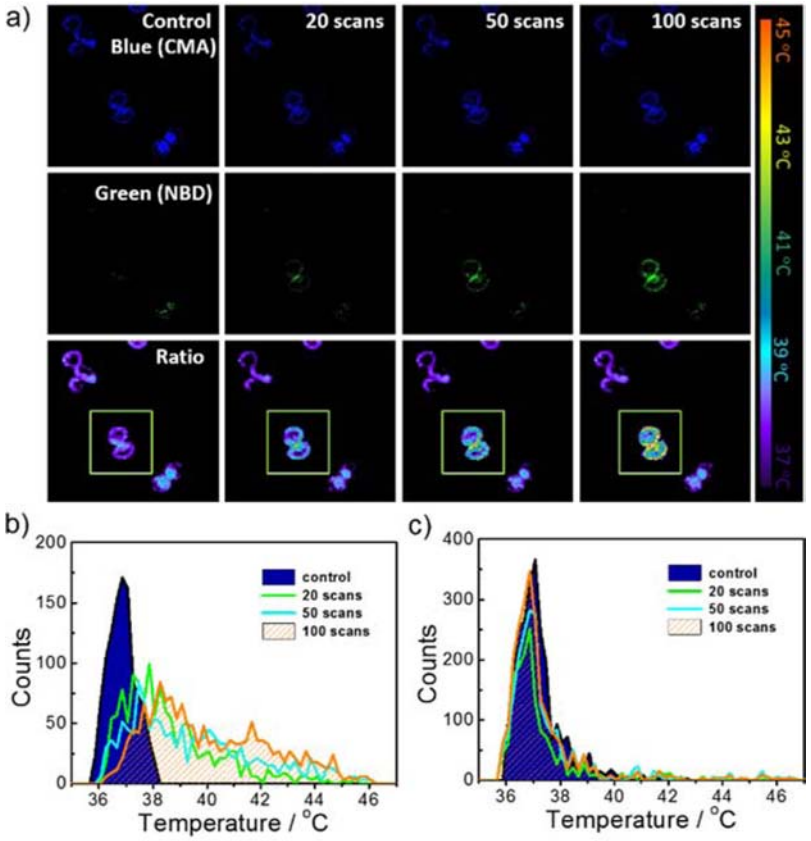

Figure 5. (a) Representative CLSM images of blue (CMA, 440 ± 20 nm) and green (NBD, 510 ± 20 nm) channels, and ratiometric images generated from green to blue channel emissions recorded for A549 cells after irradiating the green square box area with 543 nm laser for varying number of scans (20, 50, and 100 times); the cells were incubated for 2 h with **BP4** (0.35 g/L) and **BP5** (0.15 g/L) in the presence of **BP2** (0.2 g/L) micelles at first; after washing and replacing with fresh DMEM medium, the culture mixture was subjected to green light (520 nm) irradiation for 30 min and further incubation for 1.5 h. (b,c) Laser irradiation-triggered evolution of intracellular temperature gradient distributions (b) inside and (c) outside the irradiation square box area.

2,5-diphenyltetrazolium bromide (MTT), and camptothecin (CPT) were purchased from Aldrich and used as received. Fetal bovine serum (FBS), penicillin, streptomycin, and Dulbecco's modified Eagle medium (DMEM) were purchased from GIBCO and used as received. Water was deionized with a Milli-Q SP reagent water system (Millipore) to a specific resistivity of 18.4 MΩ cm. RAFT chain transfer agent, 4-cyano-4-(ethylsulfanylthiocarbonyl) sulfanylpentanoic acid (CEP),[71] fluorescence pH probe with NHS ester, 2,5-dioxopyrrolidin-1-yl 7-hydroxy-2-oxo-2*H*-chromene-3-carboxylate (7HC-NHS),[72] $^1O_2$ sensitizer, 2,2′-(anthracene-9,10-diylbis(oxy))diethanamine dihydrochloride (*An*-2NH$_2$),[65] aminoethyl methacrylamide hydrochloride (AEMA),[73] PEG$_{113}$-*b*-P(NIPAM-*co*-CMA)$_{97}$ (**BP4**),[67] and PEG$_{113}$-*b*-P(NIPAM-*co*-NBDAE)$_{95}$ (**BP5**)[67] were synthesized according to literature procedures.

Sample Preparation. *Synthesis of Eosin-Based Monomer EoS.* Eosin Y (647 mg, 1 mmol), 4-chloromethylstyrene (152 mg, 1 mmol), K_2CO_3 (275 mg, 2 mmol), and DMF (5 mL) were charged into a reaction flask, the mixture was refluxed for 6 h. After evaporating all the solvents, the residues were dissolved in CH_2Cl_2, successively washed with saturated aqueous NaCl and water, dried over anhydrous $MgSO_4$, filtered, and then concentrated on a rotary evaporator. The crude product was subjected to further purification by silica gel column chromatography using CH_2Cl_2/MeOH (98/2 v/v) as the eluent, affording 4-vinylbenzyl 2-(2,4,5,7-tetrabromo-6-hydroxy-3-oxo-3*H*-xanthen-9-yl) benzoate (EoS) as a red solid (540 mg, 67% yield). ^{1}H NMR (SI Figure S1, DMSO-d_6, δ, ppm, TMS): 8.22 (d, 1H, aromatic protons), 7.92 (m, 2H, aromatic protons), 7.42 (d, 1H, aromatic protons), 7.25 (d, 2H, aromatic protons), 6.95 (s, 2H, aromatic protons), 6.82 (d, 2H, aromatic protons), 6.62 (q, 1H, −C*H*═CH$_2$), 5.76 (d, 1H, −CH═C*H*H), 5.28 (d, 1H, −CH═CH*H*), 4.96 (s, 2H, COO−C*H*$_2$−).

*Synthesis of P(DPA-co-EoS), **P2**.* CEP (0.14 g, 0.5 mmo1), DPA (10.65 g, 50 mmol), EoS (0.15 g, 2 mmol), AIBN (0.008 g, 0.05 mmol), and 1,4-dioxane (15 mL) were charged into a reaction flask. The mixture was degassed by three freeze−pump−thaw cycles and backfilled with nitrogen. After stirring for 5 h at 70 °C, the reaction tube was quenched into liquid N_2, opened and exposed to air, and precipitated into an excess of MeOH/H_2O (1/1 v/v). The above dissolution−precipitation cycle was repeated three times. The final product was dried in a vacuum oven overnight at room temperature, yielding a reddish solid (6.6 g, yield: 61.9%). The molecular weight and molecular weight distribution of P(DPA-*co*-EoS) were determined by GPC using THF as the eluent, revealing an M_n of 16 700 and an M_w/M_n of 1.18. In combination with the M_n data determined from GPC, the chemical structure (SI Figure S2) of the product was determined to be P(DPA$_{0.95}$-*co*-EoS$_{0.05}$)$_{65}$.

Synthesis of P(DPA-co-EoS)-b-P(OEGMA-co-AEMA) Block Copolymer. **P2** macroRAFT agent (1.63 g, 0.1 mmol), OEGMA (1.37 g, 4 mmol), AEMA (0.008g, 0.05 mmol), AIBN (0.003 g, 0.02 mmol), 1,4-dioxane (6 mL), and water

DOI: 10.1021/bc500548r
Bioconjugate Chem. 2015, 26, 1328−1338

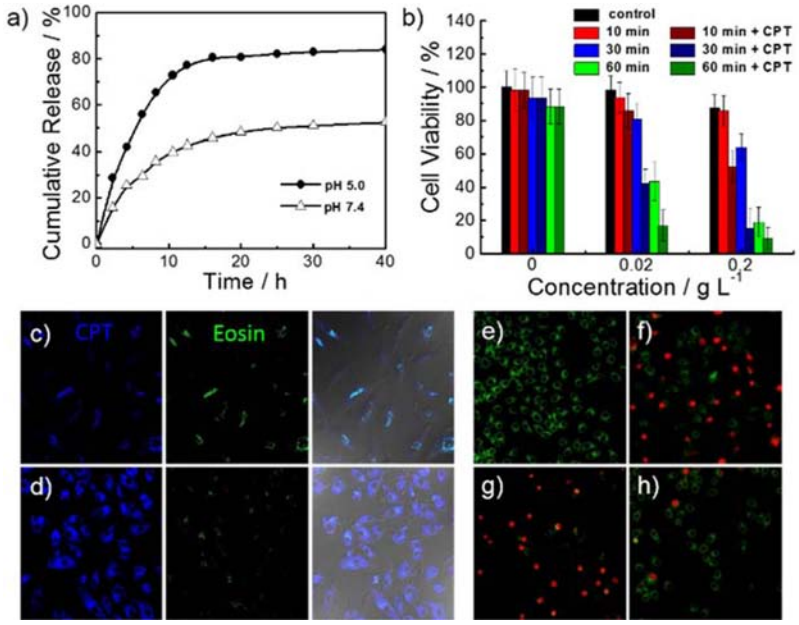

Figure 6. (a) In vitro drug release profiles of CPT-loaded **BP2** micellar solution at pH 7.4 and pH 5.0. (b) In vitro cytotoxicity determined by MTT assay against A549 cells with CPT-loaded or blank **BP2** micelles for 12 h after being subjected to green light (520 nm) irradiation for varying time periods. (c,d) CLSM images recorded for live A549 cells coincubated with CPT-loaded **BP2** micelles for 6 h after being subjected to (c) no irradiation and (d) 60 min green light irradiation (520 nm). (e–h) Apoptosis of A549 cells detected by the Live and Dead reagent (5 μM FDA, green channel at 510 ± 20 nm; 5 μM propidium iodide, red channel at 580 ± 20 nm). CLSM images of A549 cells after coincubation for 12 h in the absence (e) and (f–h) presence of (f) blank micelles and (g,h) CPT-loaded **BP2** micelles, which were first subjected to green light (520 nm) irradiation for 60 min. The addition of vitamin C as $^1O_2$ scavenger led to prominently reduced cell apoptosis (h).

(0.5 mL) were charged into a glass ampule equipped with a magnetic stirring bar. The mixture was degassed by three freeze–pump–thaw cycles and backfilled with nitrogen. After stirring for 6 h at 70 °C, the reaction tube was quenched into liquid N_2, opened, and exposed to air. The mixture was diluted with MeOH, neutralized with HCl (10 M), and precipitated into an excess of diethyl ether/acetone (2:1, v/v). The above dissolution–precipitation cycle was repeated for three times. The final product was dried in a vacuum oven overnight at room temperature to afford a yellowish solid (1.52 g, yield: 50.7%). The DP of OEGMA block was determined to be 20 by ^{1}H NMR analysis in D_2O/DCl (SI Figure S2). Thus, the polymer was denoted as P(DPA$_{0.95}$-*co*-EoS$_{0.05}$)$_{65}$-*b*-P(OEGMA-*co*-AEMA)$_{22}$.

Synthesis of P(DPA$_{0.95}$-co-EoS$_{0.05}$)$_{65}$-b-P(OEGMA-co-7HC)$_{22}$, PB3 Dual Dye-Labeled Double Hydrophilic Block Copolymers. Dual dye-labeled DHBCs, P(DPA$_{0.95}$-*co*-Eosin$_{0.05}$)$_{65}$-*b*-P(OEGMA-*co*-7HC)$_{22}$ was obtained via the amidation reaction of P(DPA$_{0.95}$-*co*-Eosin$_{0.05}$)$_{65}$-*b*-P(OEGMA-*co*-AEMA)$_{22}$ precursor with 7HC-NHS. Typically, 7HC-NHS (30 mg, 0.1 mmol), P(DPA$_{0.95}$-*co*-Eosin$_{0.05}$)$_{65}$-*b*-P(OEGMA-*co*-AEMA)$_{22}$ (0.5 g, 0.03 mmol primary amine moieties) precursor, and NEt_3 (1 mL) were added into DCM (20 mL). Then the mixture was stirred overnight at room temperature. The mixture was then passed through an alumina column using DCM as the eluent to remove salt and residual 7HC-NHS. After removal of all the solvents on a rotary evaporator, the obtained reddish solid was further purified by dialysis (cellulose membrane, molecular weight cutoff: 3500 Da) against water for 24 h, and then lyophilized as a reddish solid (0.44 g, yield: 89.3%). GPC characterization revealed an M_n of 29 700 and an M_w/M_n of 1.21. Thus, the polymer was denoted as P(DPA$_{0.95}$-*co*-EoS$_{0.05}$)$_{65}$-*b*-P(OEGMA-*co*-7HC)$_{22}$.

Fabrication of Camptothecin-Loaded Micelles. Typical procedures employed for the encapsulation of model chemotherapeutic drug, camptothecin, into polymeric micelles are as follows. **BP2** (5 mg) and camptothecin (0.5 mg) were dissolved into THF (1 mL). Then 9 mL water (pH 10) was added dropwise (9 mL/h) into the solution under vigorous stirring over 1 h. The mixture was stirred at 50 °C to remove the organic solvent. Free CPT was removed by passing through a 0.45 μm Millipore Acrodisc-12 filter. The final micellar solution was diluted with 10 mL phosphate buffer solution (PBS; 0.2 M, pH 7.4). To determine the drug loading amount, an aliquot of CPT-loaded micellar solution (1 mL) was dissolved in DMSO (9 mL). The CPT loading content was calculated to be ~6.0 wt/wt % based on the UV absorbance of camptothecin at 367 nm against a standard calibration curve.

In Vitro Photodynamic and Photothermal Efficiency Measurements. Typically, 5 mg **BP2** was dissolved in 10 mL water (pH 2), the solution pH was adjusted to the desired pH using aqueous NaOH solution (5 M). For photodynamic efficiency measurements, 1 mL of the **BP2** solution at certain pH was charged into a cuvette, 10 μL *An*-2NH$_2$ (20 mM in DMSO) was added. Then the solution was irradiated with green light (520 nm) for varying times. The *An*-2NH$_2$ concentration was quantified by measuring the fluorescene emission at 432 nm (λ_{ex} = 370 nm) against a standard calibration curve. For photothermal efficiency measurements, 1 mL of the **BP2** solution at desired pH was charged into a cuvette, the solution temperature after being subjected to green light irradiation for varying times was directly measured by a digital thermometer probe.

Photochemical Internalization Process and Photothermal Capability in Tumor Cell. The intracellular distribution of **BP3** micelles was observed with confocal laser

DOI: 10.1021/bc500548r
Bioconjugate Chem. 2015, 26, 1328–1338

scanning microscopy (CLSM). A549 cells were plated onto glass-bottom Petri dishes at a density of 80 000 cells per dish, then cultured in Dulbecco's modified Eagle medium (DMEM) with 10% fetal bovine serum (FBS), penicillin (100 units/mL), and streptomycin (100 μg/mL) at 37 °C in a CO_2/air (5:95) incubator for 24 h. **BP3** micellar solution was added at a final polymer concentration of 0.2 mg mL^{-1}. After incubation for 2 h, DMEM was replaced with fresh medium and cells were irradiated with green light (520 nm) for varying time periods, and then incubated for another period (the total time of irradiation and subsequent incubation is 2 h). Then, cells were washed with PBS three times. The images were taken using a confocal laser scanning microscopy (Leica TCS SP5 microscope).

For the photothermal potency determination within tumor cells, **BP2** micelles, **BP4**, and **BP5** were added at a final polymer concentration of 0.2, 0.35, and 0.15 mg mL^{-1}, respectively. After incubation for 2 h, DMEM was replaced with fresh medium and cells were irradiation with green light (520 nm) for 30 min, and then incubated for another 90 min. After focusing the laser to cells at low power (5% strength), the Leica software was used to define a "region of interest" (ROI, 50 μm × 50 μm square), the HeNe (543 nm) laser power was increased through software controls to 80% strength, and a single scan was performed at a scan rate of 200 Hz (corresponding to ~400 μm^2/s and 6.08 s per one scan). Then, images were taken after 20, 50, and 100 times of scanning, using low power laser (405 nm Diode laser, 5% strength).

In Vitro Drug Release Measurements. Typically, 2.5 mL camptothecin-loaded micellar solution (0.5 g/L) of **BP2** in PBS (0.02 M, pH 7.4) was placed in a dialysis tube (cellulose membrane; MWCO is 3500 Da) and then immersed into 250 mL of PBS medium (pH 7.4 or 5.0) under gentle stirring at 37 °C. Periodically, 20 mL external buffer solution was removed and replaced with equal volume of fresh medium. Upon each sampling, the 20 mL buffer solution was lyophilized and then dissolved in DMSO. The CPT concentration was then quantified by measuring the optical absorbance at 367 nm against a standard calibration curve.

In Vitro Cytotoxicity Assay. A549 cells were first cultured in Dulbecco's modified Eagle medium (DMEM) supplemented with 10% fetal bovine serum (FBS), penicillin (100 units/mL), and streptomycin (100 μg/mL) at 37 °C in a CO_2/air (5:95) incubator for 2 days. For cytotoxicity assay, A549 cells were seeded in a 96-well plate at an initial density of ca. 5000 cells/well in 100 μL of complete DMEM medium. After incubating for 24 h, DMEM was replaced with fresh medium, and the cells were treated with polymer micellar solution at varying concentrations. The treated cells were incubated in a humidified environment with 5% CO_2 at 37 °C for 24 h. Then the 96-well plate was irradiated with green light (520 nm) for varying times and then incubated for another 24 h. The MTT reagent (in 20 μL PBS, 5 mg/mL) was added to each well. The cells were further incubated for 4 h at 37 °C. The medium in each well was then removed and replaced with 150 μL DMSO. The plate was gently agitated for 15 min before the absorbance at 570 nm was recorded by a microplate reader (Thermo Fisher). Each experimental condition was done in quadruplicate and the data shown as the mean value plus a standard deviation (±SD).

Characterization. All nuclear magnetic resonance (NMR) spectra were recorded on a Bruker AV300 NMR 300 MHz spectrometer operated in the Fourier transform mode. $CDCl_3$ and D_2O were used as the solvents. Molecular weights and molecular weight distributions were determined by gel permeation chromatography (GPC) equipped with Waters 1515 pump and Waters 2414 differential refractive index detector (set at 30 °C). It used a series of two linear Styragel columns (HR2 and HR4) at an oven temperature of 45 °C. The eluent was THF at a flow rate of 1.0 mL/min. A series of low polydispersity polystyrene standards were employed for calibration. Dynamic laser light scattering (LLS) measurements were conducted on a commercial spectrometer (ALV/DLS/SLS-5022F) equipped with a multitau digital time correlator (ALV5000) and a cylindrical 22 mW UNIPHASE He−Ne laser (λ_0 = 632 nm) as the light source. Scattered light was collected at a fixed angle of 90° for duration of ~5 min. Distribution averages and particle size distributions were computed using cumulants analysis and CONTIN routines. All data were averaged over three measurements. All samples were filtered through 0.45 μm Millipore Acrodisc-12 filters to remove dust. Transmission electron microscopy (TEM) observations were conducted on a Hitachi H-800 electron microscope at an acceleration voltage of 200 kV. The sample for TEM observations was prepared by placing 10 μL of micellar solution (0.5 g/L) on copper grids coated with thin films of Formvar and carbon successively. Confocal lasers canning microscopy (CLSM) images were acquired using a Leica TCS SP5 microscope.

■ ASSOCIATED CONTENT

Ⓢ Supporting Information

NMR, UV−vis, and FL spectra, TEM and CLSM images, and DLS. This material is available free of charge via the Internet at http://pubs.acs.org.

■ AUTHOR INFORMATION

Corresponding Author

*E-mail: sliu@ustc.edu.cn.

Notes

The authors declare no competing financial interest.

■ ACKNOWLEDGMENTS

The financial support from the National Natural Scientific Foundation of China (NNSFC) Project (21274137, 51273190, 5147315 and 51033005) and Specialized Research Fund for the Doctoral Program of Higher Education (SRFDP, 20123402130010) is gratefully acknowledged.

■ REFERENCES

(1) Dolmans, D. E., Fukumura, D., and Jain, R. K. (2003) Photodynamic therapy for cancer. *Nat. Rev. Cancer 3*, 380−387.

(2) Celli, J. P., Spring, B. Q., Rizvi, I., Evans, C. L., Samkoe, K. S., Verma, S., Pogue, B. W., and Hasan, T. (2010) Imaging and photodynamic therapy: mechanisms, monitoring, and optimization. *Chem. Rev. 110*, 2795−2838.

(3) Yano, S., Hirohara, S., Obata, M., Hagiya, Y., Ogura, S.-i., Ikeda, A., Kataoka, H., Tanaka, M., and Joh, T. (2011) Current states and future views in photodynamic therapy. *J. Photochem. Photobiol. C: Photochem. Rev. 12*, 46−67.

(4) Zhu, T. C., Finlay, J. C., and Hahn, S. M. (2005) Determination of the distribution of light, optical properties, drug concentration, and tissue oxygenation in-vivo in human prostate during motexafin lutetium-mediated photodynamic therapy. *J. Photochem. Photobiol. B: Biol. 79*, 231−241.

DOI: 10.1021/bc500548r
Bioconjugate Chem. 2015, 26, 1328−1338

(5) Moore, R. B., Chapman, J. D., Mercer, J. R., Mannan, R. H., Wiebe, L. I., McEwan, A. J., and McPhee, M. S. (1993) Measurement of PDT-induced hypoxia in dunning prostate tumors by iodine-123-iodoazomycin arabinoside. *J. Nucl. Med. 34*, 405−411.
(6) Brown, J. M., and Wilson, W. R. (2004) Exploiting tumour hypoxia in cancer treatment. *Nat. Rev. Cancer 4*, 437−447.
(7) Selbo, P. K., Weyergang, A., Hogset, A., Norum, O. J., Berstad, M. B., Vikdal, M., and Berg, K. (2010) Photochemical internalization provides time- and space-controlled endolysosomal escape of therapeutic molecules. *J. Controlled Release 148*, 2−12.
(8) Norum, O. J., Selbo, P. K., Weyergang, A., Giercksky, K. E., and Berg, K. (2009) Photochemical internalization (PCI) in cancer therapy: from bench towards bedside medicine. *J. Photochem. Photobiol. B: Biol. 96*, 83−92.
(9) Berg, K., Weyergang, A., Prasmickaite, L., Bonsted, A., Hogset, A., Strand, M. T., Wagner, E., and Selbo, P. K. (2010) Photochemical internalization (PCI): a technology for drug delivery. *Methods Mol. Biol. 635*, 133−145.
(10) Nishiyama, N., Iriyama, A., Jang, W. D., Miyata, K., Itaka, K., Inoue, Y., Takahashi, H., Yanagi, Y., Tamaki, Y., Koyama, H., and Kataoka, K. (2005) Light-induced gene transfer from packaged DNA enveloped in a dendrimeric photosensitizer. *Nat. Mater. 4*, 934−941.
(11) Nomoto, T., Fukushima, S., Kumagai, M., Machitani, K., Arnida, Matsumoto, Y., Oba, M., Miyata, K., Osada, K., Nishiyama, N., and Kataoka, K. (2014) Three-layered polyplex micelle as a multifunctional nanocarrier platform for light-induced systemic gene transfer. *Nat. Commun. 5*, 3545−3549.
(12) Chen, H., Xiao, L., Anraku, Y., Mi, P., Liu, X., Cabral, H., Inoue, A., Nomoto, T., Kishimura, A., Nishiyama, N., and Kataoka, K. (2014) Polyion complex vesicles for photoinduced intracellular delivery of amphiphilic photosensitizer. *J. Am. Chem. Soc. 136*, 157−163.
(13) Shieh, M. J., Hsu, C. Y., Huang, L. Y., Chen, H. Y., Huang, F. H., and Lai, P. S. (2011) Reversal of doxorubicin-resistance by multifunctional nanoparticles in MCF-7/ADR cells. *J. Controlled Release 152*, 418−425.
(14) Lai, P. S., Lou, P. J., Peng, C. L., Pai, C. L., Yen, W. N., Huang, M. Y., Young, T. H., and Shieh, M. J. (2007) Doxorubicin delivery by polyamidoamine dendrimer conjugation and photochemical internalization for cancer therapy. *J. Controlled Release 122*, 39−46.
(15) Pasparakis, G., Manouras, T., Vamvakaki, M., and Argitis, P. (2014) Harnessing photochemical internalization with dual degradable nanoparticles for combinatorial photo−chemotherapy. *Nat. Commun. 5*, 3623.
(16) Lu, H. L., Syu, W. J., Nishiyama, N., Kataoka, K., and Lai, P. S. (2011) Dendrimer phthalocyanine-encapsulated polymeric micelle-mediated photochemical internalization extends the efficacy of photodynamic therapy and overcomes drug-resistance in vivo. *J. Controlled Release 155*, 458−464.
(17) Nikfarjam, M., Muralidharan, V., and Christophi, C. (2005) Mechanisms of focal heat destruction of liver tumors. *J. Surg. Res. 127*, 208−223.
(18) Boulnois, J.-L. (1986) Photophysical processes in recent medical laser developments: A review. *Lasers Med. Sci. 1*, 47−66.
(19) Wang, S., Huang, P., Nie, L., Xing, R., Liu, D., Wang, Z., Lin, J., Chen, S., Niu, G., Lu, G., and Chen, X. (2013) Single continuous wave laser induced photodynamic/plasmonic photothermal therapy using photosensitizer-functionalized gold nanostars. *Adv. Mater. 25*, 3055−3061.
(20) Feng, L., Wu, L., and Qu, X. (2013) New horizons for diagnostics and therapeutic applications of graphene and graphene oxide. *Adv. Mater. 25*, 168−186.
(21) Ge, Z., and Liu, S. (2013) Functional block copolymer assemblies responsive to tumor and intracellular microenvironments for site-specific drug delivery and enhanced imaging performance. *Chem. Soc. Rev. 42*, 7289−7325.
(22) Kizaka-Kondoh, S., Inoue, M., Harada, H., and Hiraoka, M. (2003) Tumor hypoxia: A target for selective cancer therapy. *Cancer Sci. 94*, 1021−1028.
(23) Narang, A. S., and Varia, S. (2011) Role of tumor vascular architecture in drug delivery. *Adv. Drug Delivery Rev. 63*, 640−658.
(24) de la Rica, R., Aili, D., and Stevens, M. M. (2012) Enzyme-responsive nanoparticles for drug release and diagnostics. *Adv. Drug Delivery Rev. 64*, 967−978.
(25) Volk, T., Jahde, E., Fortmeyer, H. P., Glusenkamp, K. H., and Rajewsky, M. F. (1993) pH in human tumour xenografts: effect of intravenous administration of glucose. *Br. J. Cancer 68*, 492−500.
(26) Gerweck, L. E., and Seetharaman, K. (1996) Cellular pH gradient in tumor versus normal tissue: potential exploitation for the treatment of cancer. *Cancer Res. 56*, 1194−1198.
(27) Barreto, J. A., O'Malley, W., Kubeil, M., Graham, B., Stephan, H., and Spiccia, L. (2011) Nanomaterials: applications in cancer imaging and therapy. *Adv. Mater. 23*, H18−H40.
(28) Lovell, J. F., Liu, T. W., Chen, J., and Zheng, G. (2010) Activatable photosensitizers for imaging and therapy. *Chem. Rev. 110*, 2839−2857.
(29) Tian, J., Ding, L., Xu, H. J., Shen, Z., Ju, H., Jia, L., Bao, L., and Yu, J. S. (2013) Cell-specific and pH-activatable rubyrin-loaded nanoparticles for highly selective near-infrared photodynamic therapy against cancer. *J. Am. Chem. Soc. 135*, 18850−18858.
(30) McDonnell, S. O., Hall, M. J., Allen, L. T., Byrne, A., Gallagher, W. M., and O'Shea, D. F. (2005) Supramolecular photonic therapeutic agents. *J. Am. Chem. Soc. 127*, 16360−16361.
(31) Koide, Y., Urano, Y., Yatsushige, A., Hanaoka, K., Terai, T., and Nagano, T. (2009) Design and development of enzymatically activatable photosensitizer based on unique characteristics of thiazole orange. *J. Am. Chem. Soc. 131*, 6058−6059.
(32) Zhu, X., Lu, W., Zhang, Y., Reed, A., Newton, B., Fan, Z., Yu, H., Ray, P. C., and Gao, R. (2011) Imidazole-modified porphyrin as a pH-responsive sensitizer for cancer photodynamic therapy. *Chem. Commun. 47*, 10311−10313.
(33) Zheng, X., Sallum, U. W., Verma, S., Athar, H., Evans, C. L., and Hasan, T. (2009) Exploiting a bacterial drug-resistance mechanism: a light-activated construct for the destruction of MRSA. *Angew. Chem., Int. Ed. 48*, 2148−2151.
(34) Torring, T., Toftegaard, R., Arnbjerg, J., Ogilby, P. R., and Gothelf, K. V. (2010) Reversible pH-regulated control of photosensitized singlet oxygen production using a DNA i-motif. *Angew. Chem., Int. Ed. 49*, 7923−7925.
(35) Cló, E., Snyder, J. W., Voigt, N. V., Ogilby, P. R., and Gothelf, K. V. (2006) DNA-programmed control of photosensitized singlet oxygen production. *J. Am. Chem. Soc. 128*, 4200−4201.
(36) He, H., Lo, P. C., and Ng, D. K. (2014) A glutathione-activated phthalocyanine-based photosensitizer for photodynamic therapy. *Chem.—Eur. J. 20*, 6241−6245.
(37) Park, S. Y., Baik, H. J., Oh, Y. T., Oh, K. T., Youn, Y. S., and Lee, E. S. (2011) A smart polysaccharide/drug conjugate for photodynamic therapy. *Angew. Chem., Int. Ed. 50*, 1644−1647.
(38) Li, F., and Na, K. (2011) Self-assembled chlorin e6 conjugated chondroitin sulfate nanodrug for photodynamic therapy. *Biomacromolecules 12*, 1724−1730.
(39) Park, S. Y., Oh, K. T., Oh, Y. T., Oh, N. M., Youn, Y. S., and Lee, E. S. (2012) An artificial photosensitizer drug network for mitochondria-selective photodynamic therapy. *Chem. Commun. 48*, 2522−2524.
(40) Lee, C. S., Park, W., Park, S. J., and Na, K. (2013) Endolysosomal environment-responsive photodynamic nanocarrier to enhance cytosolic drug delivery via photosensitizer-mediated membrane disruption. *Biomaterials 34*, 9227−9236.
(41) Hu, J. M., and Liu, S. Y. (2010) Responsive polymers for detection and sensing applications: current status and future developments. *Macromolecules 43*, 8315−8330.
(42) Zhou, K., Wang, Y., Huang, X., Luby-Phelps, K., Sumer, B. D., and Gao, J. (2011) Tunable, ultrasensitive pH-responsive nanoparticles targeting specific endocytic organelles in living cells. *Angew. Chem., Int. Ed. 50*, 6109−6114.
(43) Zhou, K., Liu, H., Zhang, S., Huang, X., Wang, Y., Huang, G., Sumer, B. D., and Gao, J. (2012) Multicolored pH-tunable and

DOI: 10.1021/bc500548r
Bioconjugate Chem. 2015, 26, 1328−1338

activatable fluorescence nanoplatform responsive to physiologic pH stimuli. *J. Am. Chem. Soc. 134*, 7803−7811.
(44) Hu, J. M., Liu, T., Zhang, G. Y., Jin, F., and Liu, S. Y. (2013) Synergistically enhance magnetic resonance/fluorescence imaging performance of responsive polymeric nanoparticles under mildly acidic biological milieu. *Macromol. Rapid Commun. 34*, 749−758.
(45) Liu, T., Hu, J. M., Jin, Z. Y., Jin, F., and Liu, S. Y. (2013) Two-photon ratiometric fluorescent mapping of intracellular transport pathways of pH-responsive block copolymer micellar nanocarriers. *Adv. Healthc. Mater. 2*, 1576−1581.
(46) Ma, X., Wang, Y., Zhao, T., Li, Y., Su, L. C., Wang, Z., Huang, G., Sumer, B. D., and Gao, J. (2014) Ultra-pH-sensitive nanoprobe library with broad pH tunability and fluorescence emissions. *J. Am. Chem. Soc. 136*, 11085−11092.
(47) Wang, Y., Zhou, K., Huang, G., Hensley, C., Huang, X., Ma, X., Zhao, T., Sumer, B. D., DeBerardinis, R. J., and Gao, J. (2014) A nanoparticle-based strategy for the imaging of a broad range of tumours by nonlinear amplification of microenvironment signals. *Nat. Mater. 13*, 204−212.
(48) Bae, Y., Fukushima, S., Harada, A., and Kataoka, K. (2003) Design of environment-sensitive supramolecular assemblies for intracellular drug delivery: polymeric micelles that are responsive to intracellular pH change. *Angew. Chem., Int. Ed. 42*, 4640−4643.
(49) Yang, X., Grailer, J. J., Rowland, I. J., Javadi, A., Hurley, S. A., Matson, V. Z., Steeber, D. A., and Gong, S. (2010) Multifunctional stable and pH-responsive polymer vesicles formed by heterofunctional triblock copolymer for targeted anticancer drug delivery and ultrasensitive MR imaging. *ACS Nano 4*, 6805−6817.
(50) Hu, X., Hu, J., Tian, J., Ge, Z., Zhang, G., Luo, K., and Liu, S. (2013) Polyprodrug amphiphiles: hierarchical assemblies for shape-regulated cellular internalization, trafficking, and drug delivery. *J. Am. Chem. Soc. 135*, 17617−17629.
(51) Parrott, M. C., Finniss, M., Luft, J. C., Pandya, A., Gullapalli, A., Napier, M. E., and DeSimone, J. M. (2012) Incorporation and controlled release of silyl ether prodrugs from PRINT nanoparticles. *J. Am. Chem. Soc. 134*, 7978−7982.
(52) Crielaard, B. J., Rijcken, C. J., Quan, L., van der Wal, S., Altintas, I., van der Pot, M., Kruijtzer, J. A., Liskamp, R. M., Schiffelers, R. M., van Nostrum, C. F., Hennink, W. E., Wang, D., Lammers, T., and Storm, G. (2012) Glucocorticoid-loaded core-cross-linked polymeric micelles with tailorable release kinetics for targeted therapy of rheumatoid arthritis. *Angew. Chem., Int. Ed. 51*, 7254−7258.
(53) Liu, G., Wang, X., Hu, J., Zhang, G., and Liu, S. (2014) Self-immolative polymersomes for high-efficiency triggered release and programmed enzymatic reactions. *J. Am. Chem. Soc. 136*, 7492−7297.
(54) Wang, X., Liu, G., Hu, J., Zhang, G., and Liu, S. (2014) Concurrent block copolymer polymersome stabilization and bilayer permeabilization by stimuli-regulated "traceless" crosslinking. *Angew. Chem., Int. Ed. 53*, 3138−3142.
(55) Wang, J., Sun, X., Mao, W., Sun, W., Tang, J., Sui, M., Shen, Y., and Gu, Z. (2013) Tumor redox heterogeneity-responsive prodrug nanocapsules for cancer chemotherapy. *Adv. Mater. 25*, 3670−3676.
(56) Colson, Y. L., and Grinstaff, M. W. (2012) Biologically responsive polymeric nanoparticles for drug delivery. *Adv. Mater. 24*, 3878−3886.
(57) Lovell, J. F., Jin, C. S., Huynh, E., Jin, H., Kim, C., Rubinstein, J. L., Chan, W. C., Cao, W., Wang, L. V., and Zheng, G. (2011) Porphysome nanovesicles generated by porphyrin bilayers for use as multimodal biophotonic contrast agents. *Nat. Mater. 10*, 324−332.
(58) Jin, C. S., Lovell, J. F., Chen, J., and Zheng, G. (2013) Ablation of hypoxic tumors with dose-equivalent photothermal, but not photodynamic, therapy using a nanostructured porphyrin assembly. *ACS Nano 7*, 2541−2550.
(59) Hu, J. M., Zhang, G. Y., Ge, Z. S., and Liu, S. Y. (2014) Stimuli-responsive tertiary amine methacrylate-based block copolymers: Synthesis, supramolecular self-assembly and functional applications. *Prog. Polym. Sci. 39*, 1096−1143.
(60) Lacey, V. K., Parrish, A. R., Han, S., Shen, Z., Briggs, S. P., Ma, Y., and Wang, L. (2011) A fluorescent reporter of the phosphorylation status of the substrate protein STAT3. *Angew. Chem., Int. Ed. 50*, 8692−8696.
(61) Fink, D. W., and Koehler, W. R. (1970) pH effects on fluorescence of umbelliferone. *Anal. Chem. 42*, 990−993.
(62) Chiefari, J., Chong, Y. K., Ereole, F., Krstina, J., Jeffery, J., Le, T. P. T., Mayadunne, R. T. A., Meijs, G. F., Moad, C. L., Moad, G., Rizzardo, E., and Thang, S. H. (1998) Living free-radical polymerization by reversible addition-fragmentation chain transfer: RAFT process. *Macromolecules 31*, 5559−5562.
(63) Liu, J., Liu, H., Boyer, C., Bulmus, V., and Davis, T. P. (2009) Approach to peptide decorated micelles via RAFT polymerization. *J. Polym. Sci., Part A: Polym. Chem. 47*, 899−912.
(64) Xu, J., Shanmugam, S., Duong, H. T., and Boyer, C. (2014) Organo-photocatalysts for photoinduced electron transfer-reversible addition-fragmentation chain transfer (PET-RAFT) polymerization. *Polym. Chem. 5*, DOI: 10.1039/c4py01317d.
(65) Arian, D., Kovbasyuk, L., and Mokhir, A. (2011) 1,9-Dialkoxyanthracene as a (1)O2-sensitive linker. *J. Am. Chem. Soc. 133*, 3972−80.
(66) Lu, H.-L., Syu, W.-J., Nishiyama, N., Kataoka, K., and Lai, P.-S. (2011) Dendrimer phthalocyanine-encapsulated polymeric micelle-mediated photochemical internalization extends the efficacy of photodynamic therapy and overcomes drug-resistance in vivo. *J. Controlled Release 155*, 458−464.
(67) Wu, Y., Hu, H., Hu, J., Liu, T., Zhang, G., and Liu, S. (2013) Thermo- and light-regulated formation and disintegration of double hydrophilic block copolymer assemblies with tunable fluorescence emissions. *Langmuir 29*, 3711−3720.
(68) Guo, J., Zhuang, J., Wang, F., Raghupathi, K. R., and Thayumanavan, S. (2014) Protein AND enzyme gated supramolecular disassembly. *J. Am. Chem. Soc. 136*, 2220−2223.
(69) Gao, F. P., Lin, Y. X., Li, L. L., Liu, Y., Mayerhoffer, U., Spenst, P., Su, J. G., Li, J. Y., Wurthner, F., and Wang, H. (2014) Supramolecular adducts of squaraine and protein for noninvasive tumor imaging and photothermal therapy in vivo. *Biomaterials 35*, 1004−1014.
(70) Kim, J. Y., Choi, W. I., Kim, M., and Tae, G. (2013) Tumor-targeting nanogel that can function independently for both photodynamic and photothermal therapy and its synergy from the procedure of PDT followed by PTT. *J. Controlled Release 171*, 113−121.
(71) Convertine, A. J., Benoit, D. S., Duvall, C. L., Hoffman, A. S., and Stayton, P. S. (2009) Development of a novel endosomolytic diblock copolymer for siRNA delivery. *J. Controlled Release 133*, 221−229.
(72) Mizukami, S., Watanabe, S., Hori, Y., and Kikuchi, K. (2009) Covalent protein labeling based on noncatalytic beta-lactamase and a designed FRET substrate. *J. Am. Chem. Soc. 131*, 5016−5017.
(73) Liu, G. H., Shi, H., Cui, Y. R., Tong, J. Y., Zhao, Y., Wang, D. J., and Cai, Y. L. (2013) Toward rapid aqueous RAFT polymerization of primary amine functional monomer under visible light irradiation at 25 degrees C. *Polym. Chem. 4*, 1176−1182.

DOI: 10.1021/bc500548r
Bioconjugate Chem. 2015, 26, 1328−1338